Precipitation Regimes during Cold-Season Central U.S. Inverted Trough Cases. Part I: Synoptic Climatology and Composite Study

ROBERT A. WEISMAN, KEITH G. MCGREGOR,* DAVID R. NOVAK,+ JASON L. SELZLER,# MICHAEL L. SPINAR, AND BLAINE C. THOMAS@

Earth Sciences Department, Saint Cloud State University, Saint Cloud, Minnesota

PHILIP N. SCHUMACHER

National Weather Service Forecast Office, Sioux Falls, South Dakota

(Manuscript received 16 October 2001, in final form 8 July 2002)

ABSTRACT

This paper is the first of two papers that examines the organization of the precipitation field in central U.S. cold-season cyclones involving inverted troughs. The first portion of the study examines the varying precipitation distribution that occurred during a 6-yr synoptic climatology of inverted trough cases. The definition of inverted trough cases has been expanded from the groundbreaking work by Keshishian et al. by 1) not requiring a closed cyclonic isobar along the frontal wave along the conventional surface front and 2) not requiring a surface thermal gradient to be present along the inverted trough. Only 8.5% of the expanded dataset produced the precipitation primarily occurring to the west of the inverted trough (''behind'' cases) as seen in Keshishian et al. The largest group of cases, comprising about 40% of the cases, produced precipitation that primarily occurred between the inverted trough and the conventional warm front (''ahead'' cases). A composite study compared a subset of the ahead cases with a subset of the behind cases. The ahead cases tended to be more progressive with a stronger jet stream located over the center of the parent low. Broad warm-air advection and frontogenesis in the lower troposphere were observed between the inverted trough and the surface warm front. Cold-air advection to the west of the inverted trough precluded the development of ''wraparound precipitation.'' In contrast, the behind cases had a stronger low-latitude wave couplet with a trough upstream of the surface low and a ridge downstream. The region of warm-air advection and frontogenesis were displaced to the west of the inverted trough and surface cyclone. In addition, the entrance region of a southwest–northeast-oriented jet streak aided the development of ascent to the west of the inverted trough while precluding the development of precipitation to the north of the conventional warm front. Thus, the inverted trough tended to act like a warm front in behind cases, as shown by Keshishian et al. Composites were also computed at both 12 and 24 h before inverted trough formation in order to generate comparisons useful to operational applications. Case study results for both ahead and behind cases will be compared with the composite cases in the companion paper.

1. Introduction

The inverted trough was identified as a frequently occurring cold-season phenomenon in the central United States by Keshishian et al. (1994, hereinafter referred to as K94). The researchers found, within a 12-yr period, 42 cases of cyclogenesis in association with an inverted trough to the lee of the Rocky Mountains (see Table 1 for case criteria). K94 determined, through a composite study, that an inverted trough was most likely to form during cyclogenesis when an area of upper-level confluence to the east of the Rockies was located over a region of lower- and middle-tropospheric ascent, often associated with warm-air advection, in the middle and lower troposphere. A typical orientation for a surface cyclone including an inverted trough is seen in Fig. 1. The trough itself actually separated two air masses: an old, modified polar air mass that was retreating toward the eastern United States (quadrant A in Fig. 1) and a fresh supply of polar or arctic air (quadrant B in Fig. 1) that is being advected southward to the east of the Rockies by a new Canadian anticyclone.

Two case studies performed by K94 showed that the frontogenesis occurring along the inverted trough reorganized the bulk of the precipitation into quadrant B

* Current affiliation: CH2M Hill, Sacramento, California.
+ Current affiliation: Atmospheric Sciences Department, University at Albany, State University of New York, Albany, New York.
# Current affiliation: Aeromet, Inc., Tulsa, Oklahoma.
@ Current affiliation: Department of Atmospheric and Oceanic Science, University of Wisconsin—Madison, Madison, Wisconsin.

Corresponding author address: Robert A. Weisman, Earth Sciences Dept., M.S. 48, Saint Cloud State University, 720 Fourth Ave. S., Saint Cloud, MN 56301-4498.
E-mail: scsweisman@stcloudstate.edu

TABLE 1. Comparison of inverted trough case criteria between this study (WO2) and Keshishian et al. (1994; K94).

	K94	WO2
Years	1974–86	1989–95
Months	Oct–Apr	Sep–Apr
Areas	Lee to 95°W	Lee to 90°W
Wind shift	50°–60°	30°
Temperature diff	5°C	None required
Consecutive maps	3	2
Cyclone	One closed isobar	None required
Cases	42	247

where the fresh arctic or polar air mass was in place at the surface. In contrast, the conventional warm front was associated with little ascent or precipitation. Dynamically, the inverted trough became a warm front that either remained stationary or propagated toward the older polar air mass in quadrant A, making it a ''backward-moving warm front.'' Cyclones in which the bulk of the precipitation falls within quadrant B as shown by K94 will be called ''behind'' cases. This alliteration is the reason that the quadrants in Fig. 1 are labeled in a counterclockwise sequence.

The role of the inverted trough as an active warm front marks a substantial departure from the classic Norwegian cyclone model (e.g., Bjerknes 1919; Bjerknes and Solberg 1922). The Structurally Transformed by Orography Model (STORM; e.g., Hobbs et al. 1996) was proposed as an adaptation of the Norwegian cyclone model to cold-season central U.S. cyclones. While the STORM does identify squall lines, the dry trough and its associated precipitation band, and the arctic front as unique to the central United States, it does not contain any surface airmass boundary along the northern half of the surface cyclone. Thus, the results of K94 added the inverted trough to the list of significant boundaries within central U.S. cyclones.

Through operational experience in the northern and central plains, the authors of this paper had observed several cold-season cyclones with inverted troughs that distorted the conventional Norwegian cyclone model precipitation distribution. However, some of these cases did not have the bulk of the precipitation in quadrant B as shown in K94. In contrast, the authors noted inverted trough systems during which precipitation primarily fell in quadrant A (Fig. 1), between the inverted trough and the conventional warm front. Cyclones with this distribution of precipitation will be called ''ahead'' cases. Also, operational experience had indicated other possible precipitation regimes. These gaps in the understanding of inverted trough cases provided the motivation for the present study.

This paper will expand on the work by K94 through two approaches: an expanded climatology and a composite study. Section 2 describes a larger climatology of inverted trough cases than that undertaken by K94 in order to document the relative frequency of ahead cases, behind cases, and other possibilities. This portion

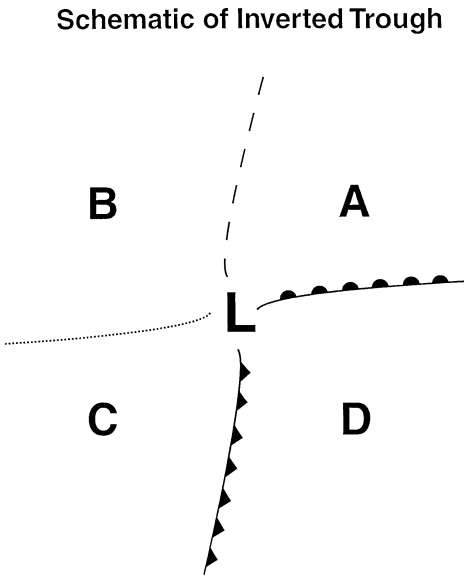

FIG. 1. Schematic diagram of central U.S. cyclone including an inverted trough (dashed line). See text for specific references for quadrants A (ahead quadrant), B (behind quadrant), C, and D.

of the study expands on the results presented in Weisman et al. (1998). Section 3 documents the results of a composite study that contrasts the processes producing precipitation in the ahead and behind cases. Section 4 discusses the results and their application to the operational forecasting problem in the central United States. Section 5 contains concluding remarks.

2. Synoptic climatology

A climatology of inverted trough cases in the central United States was performed for the six cold seasons (defined as September–April) from 1989 to 1995. The data source was the set of North American surface analyses, performed every 3 h by the National Centers for Environmental Protection (NCEP, formerly the National Meteorological Center) and made available on microfilm.

The goal of this climatology was to be more inclusive than the one performed by K94. A comparison between the climatology criteria of K94 and this study is shown in Table 1. The focus of the search was the continental United States between the eastern slopes of the Rocky Mountains and the Mississippi River (roughly between 90° and 105°W, although extending westward to 110°W in Montana). Cases of inverted troughs were limited to cyclones or frontal waves within the continental United States because of the lower density of Canadian radiosonde stations. The basic criterion was an analyzed inverted trough along the northern semicircle of a cyclone or frontal wave that existed for two consecutive map periods. Such a trough could not be previously associated with a conventional front. However, a clear wind shift of at least 30° during map periods when no trough

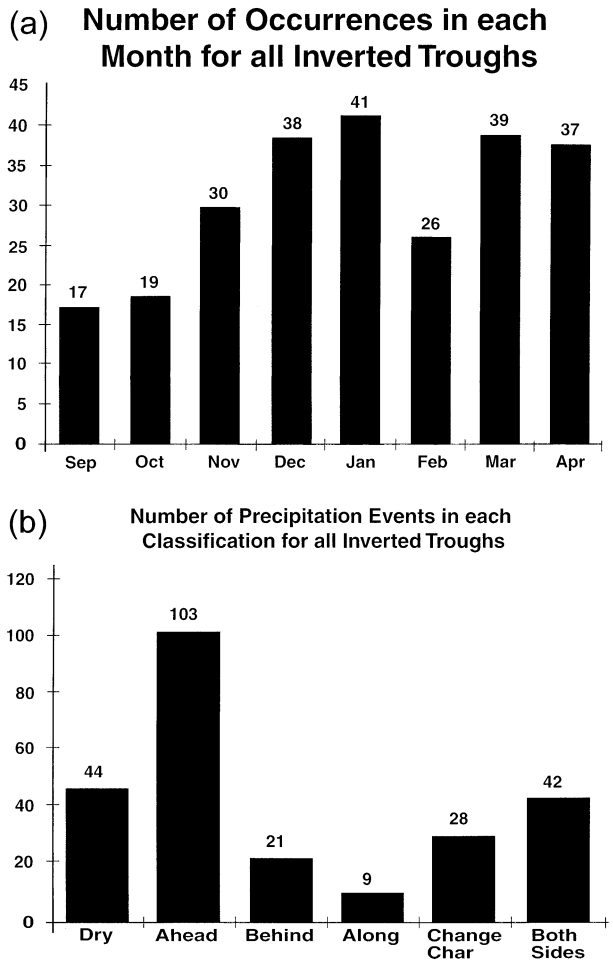

FIG. 2. (a) Monthly distribution of inverted trough cases during the 1989/90 through 1994/95 seasons. (b) Inverted trough cases by precipitation category during the 1989/90 through 1994/95 seasons. See text for definitions.

was analyzed was also included as a valid inverted trough. In contrast to K94, no temperature gradient perpendicular to the inverted trough was required in the study. Also, the requirement of a single closed cyclonic isobar was dropped. Thus, inverted troughs that met the primary polar front at a frontal wave were also included. Note that the criteria for this study are more inclusive than in K94 since the goal of this study is to examine the varying precipitation organization produced during inverted trough events rather than to focus on cyclogenesis.

A total of 247 cases, approximately 41 cases per cold season, met the criteria of this study in contrast to the 42 cases noted in the 12 yr studied by K94. The monthly distribution of cases for the six seasons shows the gradual buildup of events during the autumn months to a winter–spring plateau of 37–41 cases (Fig. 2a). Thus, the average winter–spring month exhibits six or seven inverted trough cases.

The exception to this trend is the month of February. The reduced number of February inverted trough cases cannot be solely attributed to having fewer days during the month. The relatively short duration of this study left uncertainty as to whether the low February total was a climatological fluke or the result of typical planetary-scale dynamics. Investigation of whether the February large-scale flow regime suppresses inverted troughs is beyond the scope of this study.

A stratification of inverted trough cases was performed by comparing the position of the inverted trough both with the precipitation reports on the NCEP surface analysis charts and with the echo coverage on the hourly NCEP radar summaries. The cases were then subjectively stratified into the following six categories:

1) *dry*, no measurable precipitation recorded;
2) *ahead*, clear majority of the precipitation fell in quadrant A;
3) *behind*, clear majority of the precipitation fell in quadrant B;
4) *along*, bulk of the precipitation fell within 50 km of the inverted trough (mostly along the border of quadrants A and B);
5) *both sides*, precipitation distribution relatively independent of inverted trough location; and
6) *change characteristics*, precipitation distribution begins in one of categories 2–5, but changed to at least one other category during the life cycle of the inverted trough system.

The most frequent precipitation category found for inverted trough cases in this study was ahead cases, accounting for 103 cases or 41.7% (Fig. 2b). The next most frequent were dry and both sides. Note that the behind category, which corresponds to the cases studied by K94, accounted for 21 cases (about 8.5%). However, the behind cases included some of the notorious snowfall events during the years of this study. One example is the storm of 31 October–2 November 1991, now known in Minnesota as the Halloween blizzard, that produced 71 cm of snow in Minneapolis–St. Paul, Minnesota, and 94 cm in Duluth, Minnesota. Also included as a behind case is the 1993 Thanksgiving-week Dakotas blizzard that produced snowfalls of up to 60 cm in portions of eastern South Dakota (Murtha and Blondin 1995). The two case studies in K94 (9–11 January 1975 and 13–15 April 1986) produced major South Dakota blizzards as well and would have been categorized as behind cases if they had occurred during the time period of this study. Therefore, while behind cases are far less frequent than ahead cases, these storms also require attention.

Since the goal of this study was to focus on the ahead and behind cases, other case categories were set aside. The authors hypothesized that the change-characteristics category involved precipitation regimes that are hybrids of the ahead, behind, and along categories during the life cycle of the storm. Thus, a successful forecast of these hybrid cases would involve a combination of the

conceptual model developed here as well as the Norwegian cyclone model. The dry cases were dropped since they could be in any other category that would become evident if sufficient moisture or lift was present. The both-sides cases were set aside since they either seemed to be hybrids of both the ahead and behind patterns or the precipitation showed little deviation from the Norwegian cyclone model. Therefore, the remainder of this study will focus on the key differences between ahead and behind cases. This is the goal of both the compositing study performed in this paper and the case studies to be performed in a future paper.

3. Composite study

a. Methods and data

Composite studies have advantages and weaknesses. The major weakness is that mesoscale features crucial to the development of the individual storm or precipitation maximum get lost when they are averaged with many other cases. Even if some mesoscale features such as jet streaks, deformation zones, and fronts do recur among several cases, their strength can be reduced or even lost because of the compositing process. This loss is especially likely if mesoscale features appear in different locations relative to the cyclone or inverted trough during individual cases. Such a smearing effect has been documented by several researchers (e.g., Lackmann et al. 1996). However, the composite approach will allow the most important synoptic and meso-α-scale features that are shared among the cases to become apparent. In fact, Mullen and Baumhefner (1988) noted, in their study of explosive cyclogenesis, that key processes found to be crucial to the development of individual cyclones were not as important to the average explosive cyclone. Therefore, the authors recommended that both case studies and composite studies be performed in order to truly understand a weather system. Thus, the composite study, which highlights differences between ahead and behind cases, is being presented here.

To ensure the best possible results from the individual ahead and behind composites, the 6-yr climatology of inverted trough cases described in section 2 was winnowed in order to identify ''clean'' ahead and ''clean'' behind cases for which no precipitation occurred on the opposite side of the inverted trough. A total of 19 ahead cases and 5 behind cases from the 6-yr period met this criterion (Table 2). Upper-air observations, the basis of the composite, were obtained from the *Radiosonde Data of North America* CD-ROM produced by Forecast Systems Laboratory and the National Climatic Data Center. If a case continued for more than one time period, then the subsequent time periods were also used in the computation. Thus, the ahead (behind) cases selected encompassed 33 (9) regular radiosonde observing periods. There was no composite computed for 12 h after inverted trough formation as was performed in K94.

TABLE 2. Radiosonde time periods and cyclone positions used in compositing study. Origin location is the position of the cyclone/frontal wave, rounded to the nearest degree, during the first radiosonde period in which the surface inverted trough was analyzed.

Starting time and date	Time periods	Origin lat (°N)	Origin lon (°W)
Ahead			
0000 UTC 16 Jan 1990	1	38	104
1200 UTC 23 Jan 1990	1	39	95
1200 UTC 13 Apr 1990	2	40	95
1200 UTC 18 Sep 1990	2	37	100
0000 UTC 3 Dec 1990	1	35	96
0000 UTC 17 Dec 1990	3	37	105
0000 UTC 17 Mar 1991	1	35	104
0000 UTC 19 Apr 1991	2	36	92
0000 UTC 24 Sep 1991	1	42	99
1200 UTC 13 Mar 1992	2	46	99
1200 UTC 1 Nov 1992	1	37	95
1200 UTC 20 Mar 1993	1	27	96
0000 UTC 30 Mar 1993	3	38	98
0000 UTC 11 Apr 1993	2	40	95
1200 UTC 23 Apr 1993	2	42	102
1200 UTC 19 Sep 1993	3	37	99
1200 UTC 4 Nov 1993	1	45	98
0000 UTC 27 Nov 1994	3	38	104
0000 UTC 9 Dec 1994	1	32	95
Behind			
1200 UTC 28 Sep 1990	1	45	105
1200 UTC 31 Oct 1991	3	32	94
1200 UTC 6 Dec 1992	3	27	94
1200 UTC 19 Mar 1993	1	35	95
1200 UTC 25 Apr 1995	1	45	105

A wide range of air masses could have been involved in the individual inverted trough cases. This is a result of both the 9-month period involved in the search and the climatological variation within each cold season. The resulting composites could not be expected to involve the same average air mass in both the ahead and behind cases. For this reason, direct temperature comparisons are not made between ahead and behind composites; the focus is on baroclinic zones and frontogenesis locations.

Since only nine clean behind time periods were found within the 6-yr dataset, the behind composites were noisier than the ahead composites. The authors realize that the lack of cases is responsible for much of the noise. Also, this approach sacrificed the ability to compute the statistical significance of the differences between the two composite sets. However, the introduction of hybrid cases would add signals not common to all behind cases. The authors feel that the restriction of using only ''clean'' time periods in the composite produced meaningful synoptic-scale differences between the ahead and behind composites, which was the primary goal of this study.

The surface positions of the inverted troughs and their associated cyclones or frontal waves selected for compositing are shown in Fig. 3. Note that the positions of the inverted trough cases selected for compositing spanned the area from the Canadian border to the Gulf

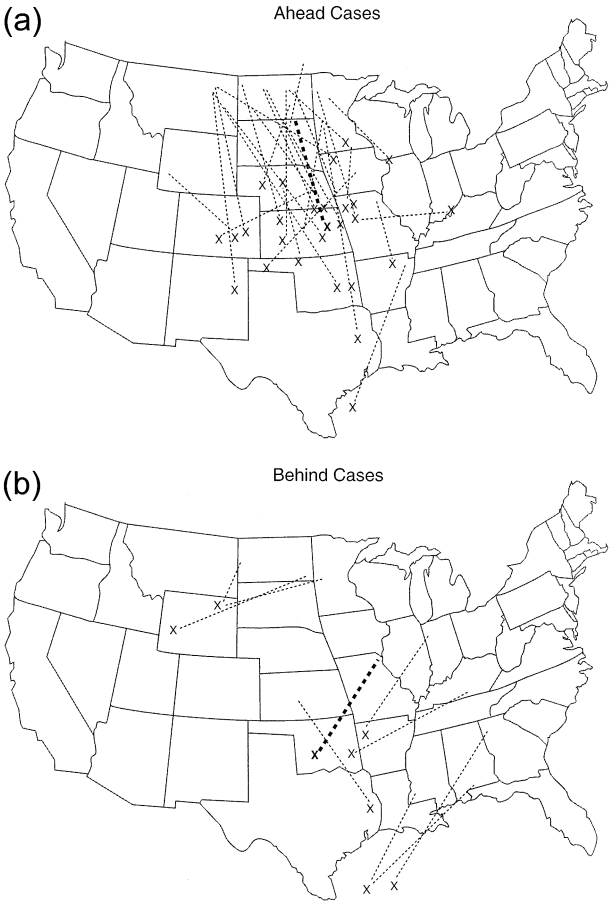

FIG. 3. (a) Cyclone/frontal wave (shown by X) and inverted trough positions (shown by dashed line) for all ahead cases used in composite study. The mean ahead inverted trough location is shown by the boldface dashed line and X. (b) As in (a) but for behind cases.

of Mexico coast. Some of the cyclone/frontal wave positions (noted by X) have multiple inverted trough positions. This occurred because these cases spanned multiple time periods. In these cases, the inverted troughs rotated relative to the cyclone/frontal wave. This phenomenon has been noted in several hybrid cases by the authors and will be the subject of future work.

Also, note that the inverted trough could extend northwestward, northward, or northeastward from the cyclone/frontal wave. For this reason, an inverted-trough-relative coordinate system was required for the composite. In this coordinate system, the cyclone or junction point between the inverted trough and the nearby front at the first radiosonde time after inverted trough formation was defined as the origin. The inverted trough was defined as lying along the positive y axis. Thus, in Fig. 1, the positive y axis would lie along the inverted trough, the negative x axis would separate quadrants B and C, the positive x axis would separate quadrants A and D, and so on.

In order to place each case within the inverted-trough-relative coordinate system, the following computations were performed for each time period:

1) All radiosonde observations within 20° latitude and 20° longitude of the cyclone/frontal wave were identified.
2) The rotation angle of the inverted trough relative to true north within the meteorological coordinate system was computed. This determined the rotation angle for the trough-relative coordinate system at this time.
3) The position of the surface cyclone/frontal wave was redefined as the origin.
4) New (x, y) coordinates (in kilometers) within the inverted-trough-relative system were computed for all radiosonde observations based on each observation's perpendicular distance from the new y axis (inverted trough) and the new x axis.
5) Each wind observation was reexpressed as trough-normal (x direction) and trough-parallel (y direction) components. Thus, the final wind directions are also trough relative in order to determine divergence and frontogenesis relative to the inverted trough.
6) The two wind components, as well as temperature, dewpoint, and geopotential, were interpolated onto a vertical grid having 19 layers at 50-hPa intervals between 1000 and 100 hPa.
7) After all observations for the time period had been ingested, a Barnes (1964, 1973) analysis of the five variables listed in step 5 was performed at each 50-hPa level in order to define these variables every 100 km within a 5000 km by 5000 km trough-relative coordinate system.

After the three-dimensional grid was defined for each time period, the average value among the cases was determined at each grid point in the trough-relative coordinate system for both the ahead and the behind cases. The five averaged fields generated in step 5 above were then subjected to a final Barnes smoothing to eliminate noise generated by the averaging process. The results included temperature, dewpoint temperature, trough-relative wind velocity, and geopotential height fields at 50-hPa intervals. Significant signals in the temperature and wind fields did survive the compositing process and will be shown in section 3b. However, the composite fields frequently depicted height fields on isobaric surfaces whose implied wind direction deviated greatly from the geostrophic. The most probable reason for this is the key role that split middle- and upper-tropospheric flow plays in the development and maintenance of the inverted trough as seen in K94. Thus, streamlines and isotachs, rather than height contours, will be used to depict the wind field.

Derived quantities were computed from the five basic smoothed variables. These included divergence, vorticity, and the two forcing functions of the quasigeostrophic (QG) omega equation, temperature advection and relative vorticity advection. Note that relative vorticity was

substituted for absolute vorticity since the latitude of any gridpoint term was uncertain after the coordinate transformation and averaging. Two-dimensional adiabatic frontogenesis was also computed for each level using the total wind after Miller (1948). Vertical velocities were computed using the kinematic method (Bellamy 1949) with the application of the O'Brien (1970) correction. No additional smoothing was performed on these derived fields. Also, isentropic fields were calculated for selected levels of the ahead and behind composites. These analyses make up the composites for the ahead 0-h and behind 0-h periods.

In order to note differences in development for use in forecasting applications, composites were also made for the 19 ahead radiosonde time periods and the 5 behind radiosonde time periods that preceded the initial appearance of the inverted trough. These time periods preceded the times listed in Table 2 by 12 h. Composites from the earlier time period are designated the ahead − 12 h (behind − 12 h) composites. Composites were also computed for the previous radiosonde period to produce ahead − 24 h (behind − 24 h) composites. Note that, in figures depicting the −12 h and −24 h periods, the 0-h surface position of the inverted trough and cyclone/frontal wave is shown, rather than the current position.

Because of transformation of the data to an inverted-trough-relative coordinate system, the *y* axis is not directed toward the north. The mean orientation of the *y* axis is shown by the bold average inverted trough position in Fig. 3a (ahead) and Fig. 3b (behind). Although directions are noted in the subsequent figures depicting the composite results, all directions noted are within the inverted-trough-relative coordinate system and do not exactly correspond to geographic directions.

b. Composite results

Some differences in development between ahead and behind cases became evident in the composite isobaric analyses 24 h before inverted trough development. The 850 hPa ahead − 24 h (Fig. 4a) analysis showed a trough–ridge pair with the base of the trough centered about 1600 km west of the eventual surface low. A ridge axis was present near the location of the eventual inverted trough so that weak warm-air advection could already be inferred near the *y* axis (thick dashed line). There was also evidence of split flow along the northern edge of quadrant A (see Fig. 1 for reference locations). However, mainly zonal flow is seen at this time period at 700 hPa (Fig. 4b) and higher levels (not shown).

For the behind − 24 h composites, the 850-hPa flow pattern was diffuse with a warm-core low near the boundary of quadrants C and D (not shown). At higher levels, split flow appeared at all levels of the behind − 24 h composite (Figs. 5a,b) and was farther south than in the ahead cases. An implied dilatation axis was noted 400–800 km to the west of the future in-

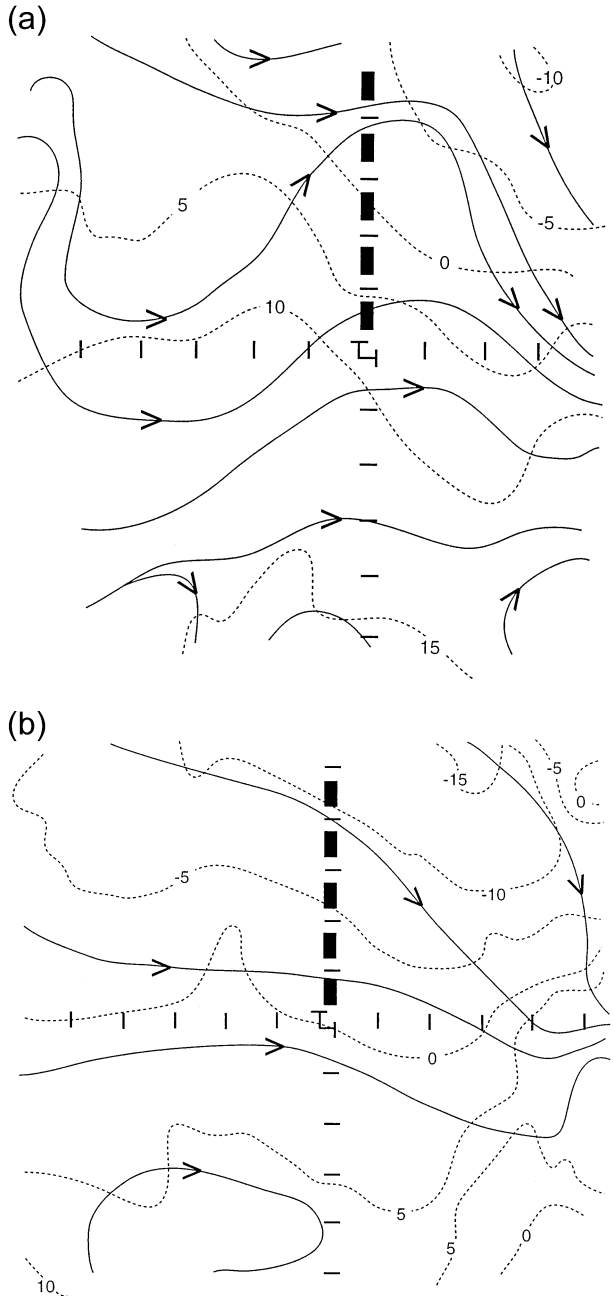

FIG. 4. Composite ahead − 24 h isobaric analysis at (a) 850 and (b) 700 hPa. Note that the position of the cyclone/frontal wave at the time of inverted trough development is depicted by the L and the eventual inverted trough position along the $+y$ axis is shown by the bold dashed line. Tick marks are plotted along the axes every 400 km. Isotherms (every 5°C) are shown as thin dashed lines. Streamlines are shown as thin solid lines with arrows. Isotachs (selected intervals) are shown as bold solid (dashed) lines at 10 (5) m s^{-1} increments. Wind speed maxima are depicted with a bold J. Absence of isotachs indicates that all wind speeds are <10 m s^{-1} at all levels below 500 hPa and <25 m s^{-1} at levels from 500 hPa and higher.

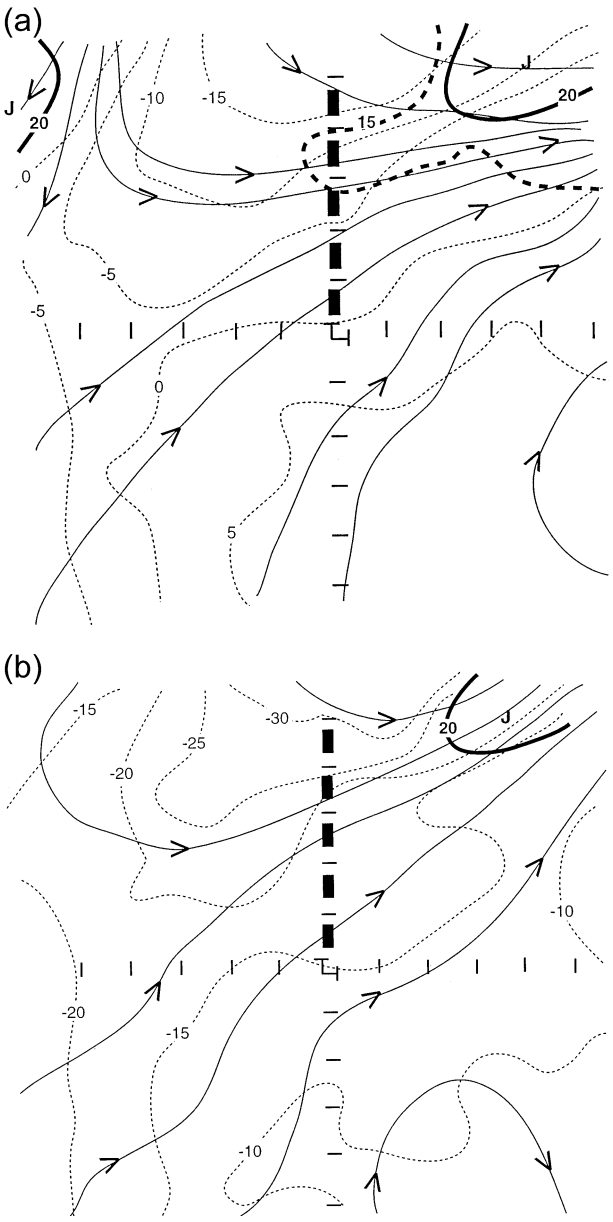

FIG. 5. Composite behind − 24 h isobaric analysis as in Fig. 4 at (a) 700 and (b) 500 hPa. Tick marks are plotted along the axes every 400 km. Isotherms (every 5°C) are shown as thin dashed lines. Streamlines are shown as thin solid lines with arrows. Isotachs (selected intervals) are shown as bold solid (dashed) lines at 10 (5) m s^{-1} increments. Wind speed maxima are depicted with a bold J. Absence of isotachs indicates that all wind speeds are <10 m s^{-1} at all levels below 500 hPa and <25 m s^{-1} at levels from 500 hPa and higher.

verted trough in quadrant B at 700 hPa (Fig. 5a). This same feature was displaced farther to the north at 500 hPa (Fig. 5b). Wind speeds were weak at this time (the lack of isotachs indicate that all wind speeds are less than 10 m s^{-1}), probably since the location of the dilatation axis actually varies in the individual cases. The flow in quadrant A was characterized by confluence at all levels, with a more organized southwesterly flow in the southern stream than was seen in the ahead composite. The 850-hPa warm-air advection seen in the ahead − 24 h composite was absent in the behind − 24 h composite, a sign that frontogenesis had yet to develop despite confluent flow.

The 500-hPa flow hinted at a jet streak entrance region, which was verified by speeds of at least 25 m s^{-1} evident at 200 hPa (not shown). A straight jet streak would have produced upper-air divergence and, therefore, the lowering of surface pressure near the eventual position of the surface low and inverted trough (Uccellini and Johnson 1979). Such a jet entrance region just downwind of the location of the future inverted trough was also noted by K94. No such jet was seen in the ahead − 24 h composite.

The 850-hPa short-wave trough within the ahead − 12 h composite (Fig. 6a) was located about 800 km to the west of the future inverted trough position (note again that the marked trough would not develop until the next radiosonde period). A broad area of warm-air advection was implied from the current 850-hPa trough position into quadrant A. However, the calculation of temperature advection (not shown) showed a distinct maximum from along the future inverted trough to about 400 km to the east and southeast of the future cyclone (near the *x* axis and into quadrant D). The reason for the concentration of the warm-air advection to the east and southeast of the future cyclone was the 10 m s^{-1} isotach in the same position, weakly indicating the possibility of a low-level jet stream.

The enhanced warm-air advection near the wind maximum, surrounded by weaker warm-air advection, produced a maximum of frontogenesis at this level (not shown). A frontogenesis maximum would induce a direct thermal circulation in which the warm air in the vicinity of the maximum rises and the cold air sinks (e.g., Bluestein 1986; Keyser et al. 1988). The rising branch of the circulation would tend to slope over the colder air with height. Thus, the presence of frontogenesis would be consistent with the formation of a warm front near the boundary of quadrants A and D.

A weak trough developed at 700 hPa (Fig. 6b), also producing weak warm-air advection over the future inverted trough and slightly into quadrant A. This warm-air advection also led to some modest frontogenesis just to the east of the future inverted trough position (not shown), in roughly the same position as at 850 hPa. Last, note that cold-air advection was implied at both 850 and 700 hPa behind the −12 h positions of the troughs at those levels.

A flat trough–ridge pair was seen at 500 and 300 hPa (Figs. 6c,d). Note the relative lack of tilt upstream with height as the base of the trough at all levels was about 800 km upstream of the future inverted trough. In fact, the system was nearly vertical through all layers. This also implies that there would be cyclonic vorticity ad-

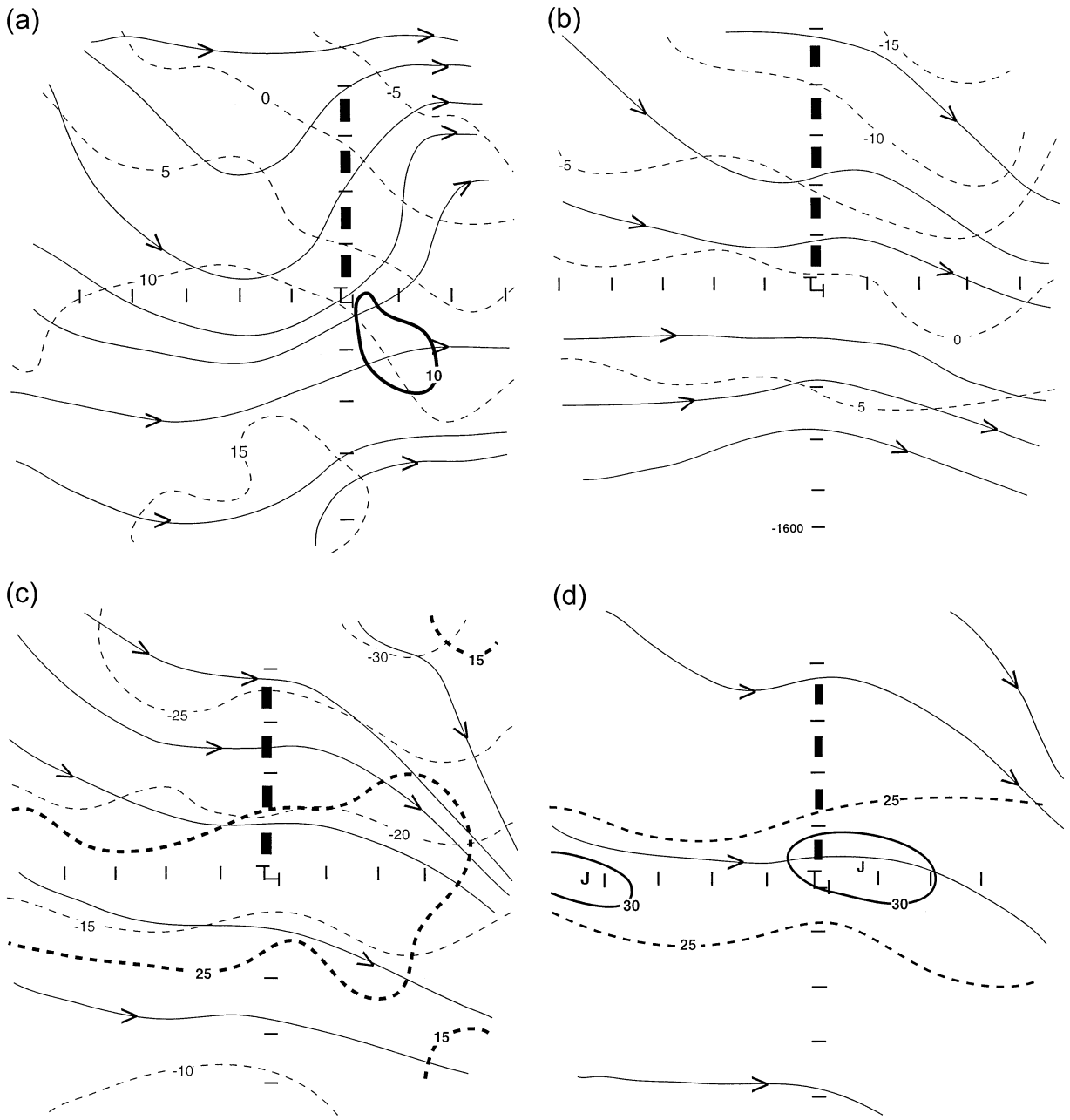

FIG. 6. Composite ahead − 12 h isobaric analysis as in Fig. 4 at (a) 850, (b) 700, (c) 500, and (d) 300 hPa.

vection over the future position of the inverted trough and cyclone, but the calculation produced a noisy signal at this time (not shown).

In the upper troposphere, a jet streak was noted along the *x* axis. The wind speeds were 25 m s^{-1} at 500 hPa and 30 m s^{-1} at 300 hPa. Note that these velocities would be underestimates from individual cases because of the slightly varying position of the jet maxima. The position of the jet near the future cyclone would tend to indicate rapid progression of the system to the east. Note that the ahead quadrant, by straight-jet dynamics (Uccellini and Johnson 1979), would be favored for ascent due to divergence aloft. The divergence field at 300 hPa (not shown) was actually maximized from the future low position up to about 400 km westward. Thus, either the divergence field may have been responding to an upward increase of cyclonic vorticity advection or the jet-streak-induced divergence resembled the cyclonically curved jet case examined by Moore and VanKnowe (1992).

The behind − 12 h composites had a markedly different signal. At 850 hPa (Fig. 7a), the trough, which

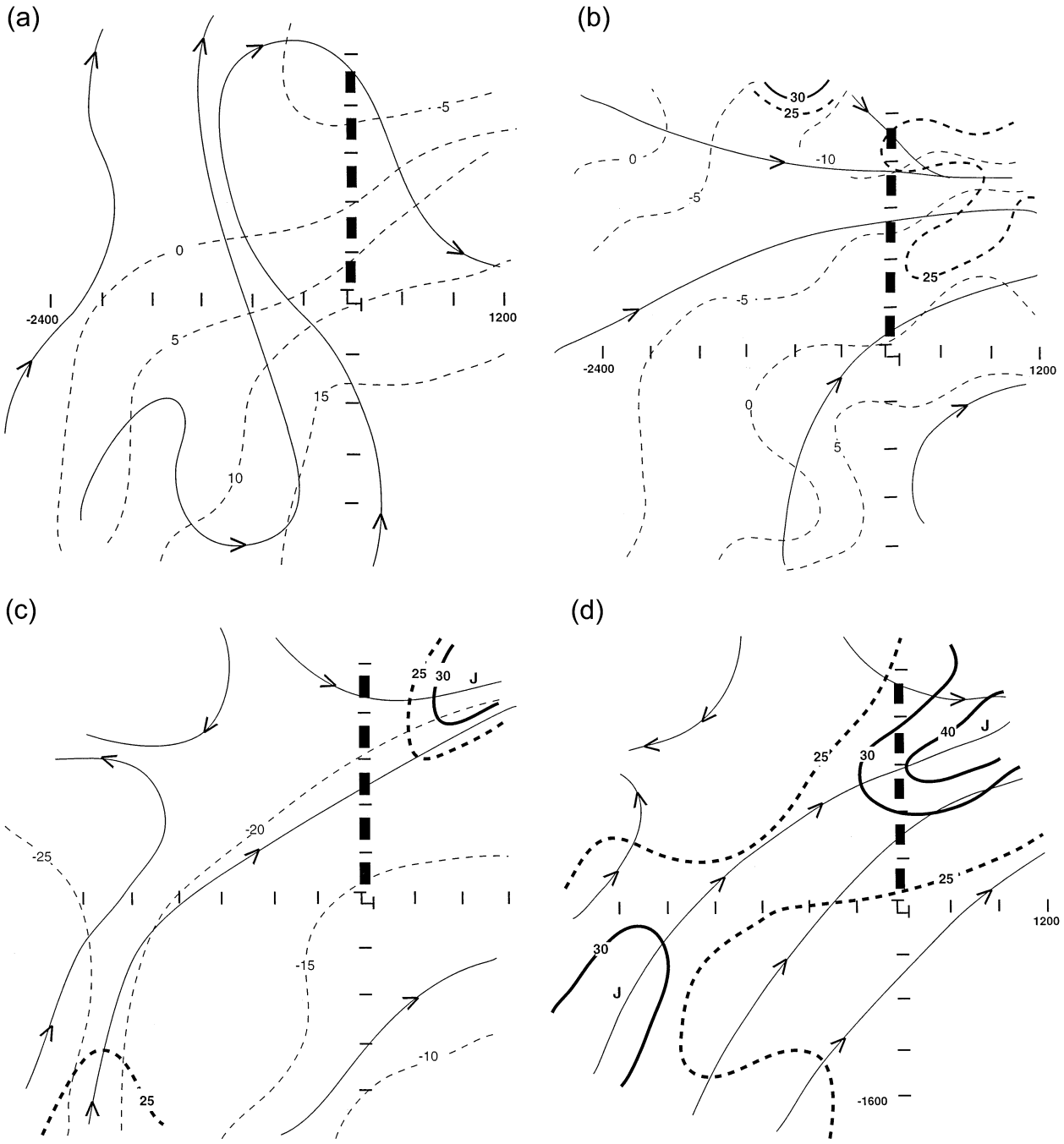

FIG. 7. Composite behind − 12 h isobaric analyses as in Fig. 4 at (a) 850, (b) 700, (c) 500, and (d) 300 hPa.

will initiate the inverted trough 12 h later, was located nearly 2000 km southwest of the future surface cyclone. A highly amplified ridge was located over the position of the future inverted trough. The strongest warm-air advection and implied frontogenesis (not shown) were primarily focused 400–800 km to the west of the future trough. Not only did this frontogenesis favor lift in quadrant B, but it also forced the isotherms, nearly perpendicular to the future inverted trough at −12 h, to rotate parallel to the future trough.

At 700 hPa (Fig. 7b), split flow was noted similar to 12 h earlier, but the streamlines to the south of the *x* axis were far more anticyclonically curved than 12 h earlier. The streamlines did not show a trough, but there was a thermal trough in quadrant C about 1400 km southwest of the future cyclone. In contrast, the iso-

therms and the streamlines are nearly parallel to the east of the confluence zone in quadrant A. Therefore, most of the warm-air advection at this level (not shown) was limited to quadrant B.

At 500 hPa (Fig. 7c), two distinct flows were seen with an axis of dilatation about 1200 km north of the *x* axis in Quadrant B. A jet streak entrance region was seen in quadrant A and another speed maximum was entering the domain from the southwest. A distinct short wave was not seen in the streamline field; however, there was a cold-air pocket in quadrant C, 1200 km southwest of the origin. The existence of this cold-air pocket was confirmed by a weak cyclonic relative vorticity maximum (not shown).

The jet streak velocities in quadrant A strengthened at 300 hPa (Fig. 7d). The isotachs extended into quadrant B, which was farther west than during the previous period. Also, the southerly portion of the split flow began to dominate the composite domain, so that the right entrance region of the jet streak was over the region of low-level frontogenesis within quadrant A.

Within the ahead 0-h composite, the lower-tropospheric levels (Figs. 8a,b) were similar to 12 h before, except that the trough had progressed so that the 850- and 700-hPa troughs were directly above the surface inverted trough. Since the trough was nearly vertical, all of the warm-air advection occurred in quadrant A while cold-air advection was seen in quadrant B (Fig. 9a). This accounted for the cessation of precipitation to the west of the inverted trough. Both the 850- and 700-hPa levels exhibited wind maxima near the streamline trough, which intensified the warm-air advection along the *x* axis within 800 km of the surface cyclone. Thus, an active warm front, as depicted in the Fig. 1 schematic, had formed. A cross section of the temperature advection near the *x* axis (Fig. 9b) showed that the inverted trough marked the boundary between warm-air and cold-air advection throughout the troposphere, with the strongest warm-air advection in the lowest 250 hPa.

The contrast of the low-level wind maximum with lower wind speeds farther to the north produced consistent frontogenesis within quadrant A through 500 hPa (Figs. 10a,b). Note that, at 500 hPa (Fig. 10b), there is a weaker axis of frontogenesis along the inverted trough as well. A cross section (Fig. 10c) showed that the strongest frontogenesis was located 400–1200 km to the east of the inverted trough, with the maximum at 500 hPa. Note that there was a secondary frontogenesis maximum 500 km to the west of the inverted trough centered at 300 hPa. However, this maximum was situated above strong cold-air advection (see Figs. 9a,b). While this would induce another direct thermal circulation, lower-tropospheric sinking and drying prevented the rising branch of the upper-tropospheric circulation from producing precipitation.

At 500 hPa (Fig. 8c), the streamline trough had progressed to within 200–400 km of the inverted trough. The zonal wind maximum was located very close to the surface cyclone, supporting the more progressive nature of the ahead cases. There was little change at jet level (Fig. 8d), except that the maximum winds had reached 30 m s^{-1} at 300 hPa. The orientation of the 300-hPa jet streak appears to be cyclonically curved. Moore and VanKnowe (1992) demonstrated that the region to the left of a cyclonically curved jet streak downwind of the wind maximum is favored for ascent. The 300-hPa divergence field (Fig. 11) showed a divergence maximum within 200 km in quadrant A and downwind of the jet maximum. Thus, the divergence field was consistent with the Moore and VanKnowe (1992) interpretation. Note that the position of the jet-streak-forced divergence was nearly above the lower-tropospheric frontogenesis maximum. The collocation of these two forcing mechanisms is consistent with the key processes shown during inverted trough cyclones by K94.

The stronger winds at 300 hPa did allow a modest amount of relative vorticity advection (Fig. 12a) in quadrant A within 400 km of the surface inverted trough. A vertical cross section of relative vorticity advection (Fig. 12b) showed that the maximum cyclonic vorticity advection is concentrated in the upper troposphere, resulting in an upward increase of cyclonic vorticity advection, the actual forcing term within the QG omega equation, in quadrant A just ahead of the inverted trough. However, note that there is very little positive vorticity advection (PVA) in the middle troposphere.

The ascent forcing shown from vorticity advection is also located over the same area with the maximum lower-tropospheric warm-air advection and frontogenesis. As a result, the 500-hPa kinematic vertical velocity (Fig. 13a) showed ascent within 400 km of the surface inverted trough with an extension out to 800 km just south of the *x* axis. The cross section of the vertical velocity (Fig. 13b) showed that the ascent was maximized within the middle troposphere despite what appeared to be little PVA at this level.

In the behind 0-h composite, the 850-hPa ridge (Fig. 14a) had amplified since the previous composite and shifted into quadrant A. One trough remained far to the south of the surface cyclone. The highly amplified trough–ridge pair produced a southeasterly flow near the surface inverted trough (*y* axis). This produced a maximum in the warm-air advection above the surface inverted trough with a small portion in quadrant B (Fig. 15a). This is a dramatic change from the ahead 0-h composite. Another trough was propagating through the southwest flow in quadrant B. The persistent southwest flow had rotated the isotherms from the previous time period so that they were more parallel to the surface inverted trough up to 400 km into quadrant B. This is consistent with the surface inverted trough acting as the dominant warm front during behind cases. Also, the strongest winds were seen where the flow crossed the surface trough into quadrant B. The prolonged period of lift as the flow moved into quadrant B resulted in

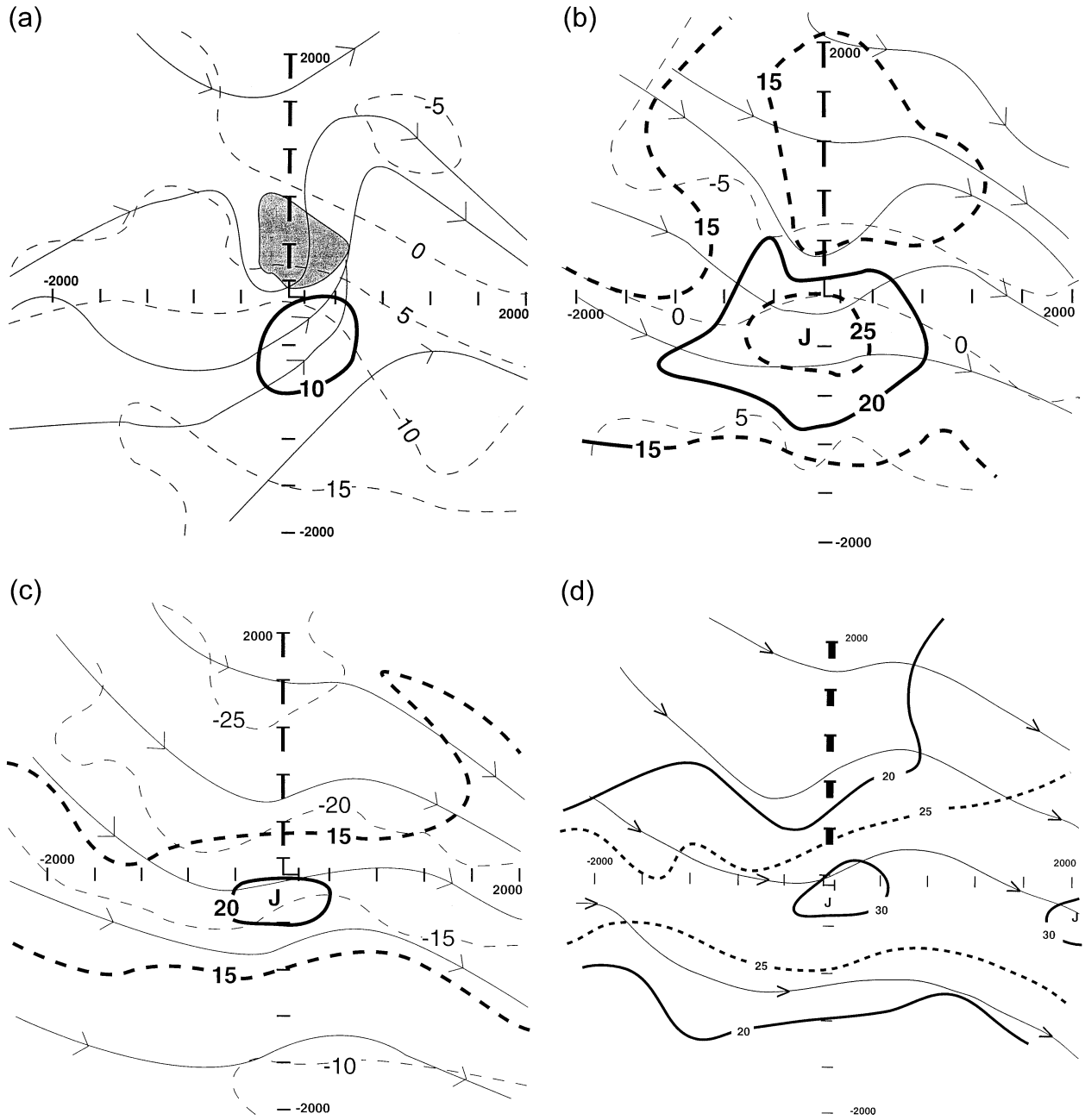

FIG. 8. Composite ahead 0-h isobaric analysis as in Fig. 4 at (a) 850, (b) 700, (c) 500, and (d) 300 hPa. Note that the stippled area at 850 hPa indicates areas with a dewpoint depression of ≤5°C. The lack of stippling in (b)–(d) indicates that all areas have a dewpoint depression >5°C.

near-saturation as represented by the stippled area in Fig. 14a.

At 700 hPa (Fig. 14b), the streamline trough in quadrant B was the dominant feature with warm-air advection within 400 km of the surface inverted trough. Note also that the streamlines depicted a tilt of the trough farther west with height, in contrast to the ahead cases. The warm-air advection at both lower-tropospheric levels (Figs. 15a,b) was much more focused along the inverted trough than in the ahead cases. The cross section (Fig. 15c) showed that the strongest warm-air advection was located near the surface inverted trough position in the lowest layers, but tilted into quadrant B above 700 hPa. Also, a second warm-air advection maximum appeared between 800 and 1200 km in quadrant B. The signal was noisy because of the low number of cases as mentioned in section 3a. This led to several frontogenesis maxima within quadrant B (not shown).

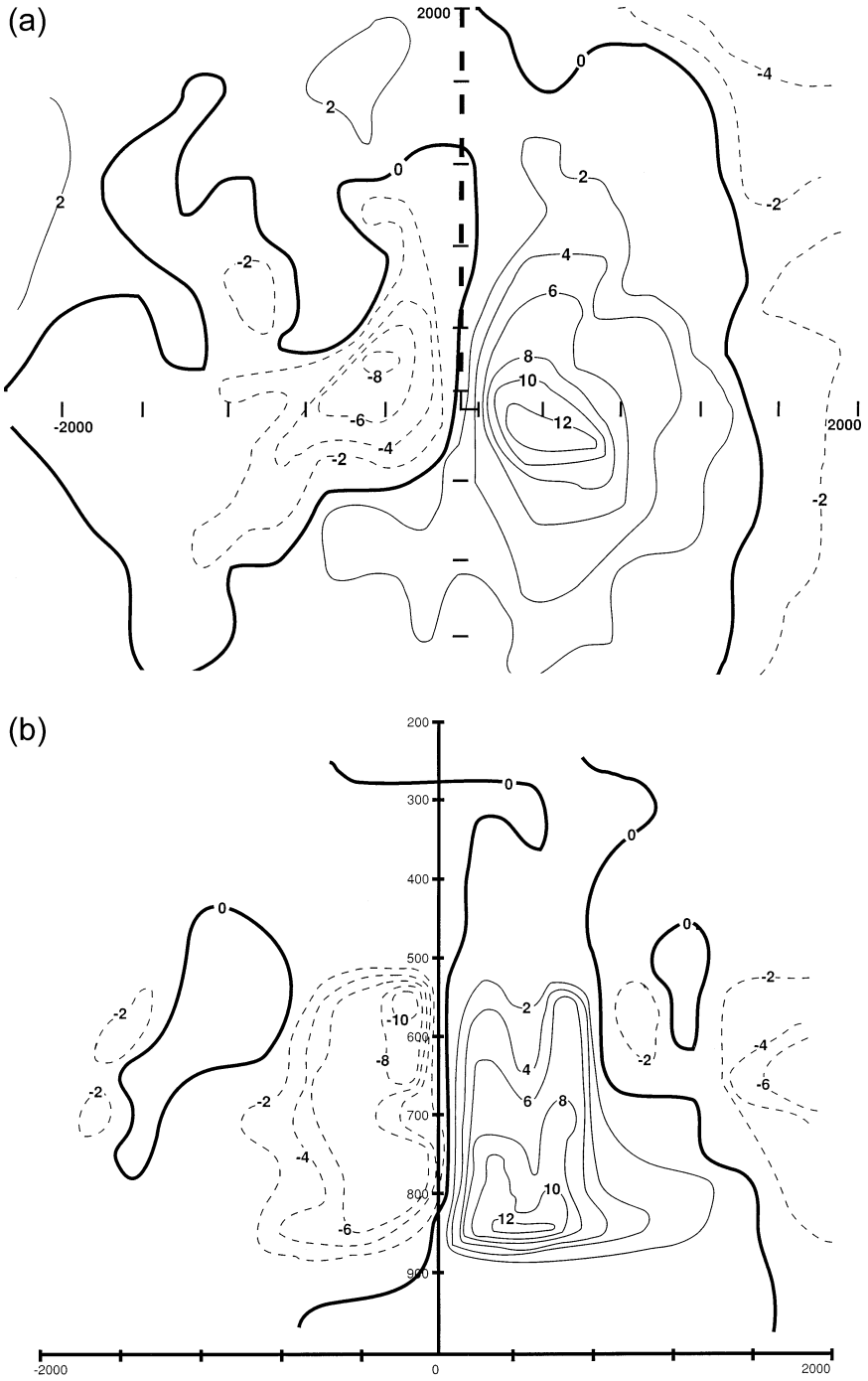

FIG. 9. (a) Isobaric temperature advection (10^{-8} K s^{-1}) for the ahead 0-h composite at 850 hPa. Warm-air (cold air) advection is denoted by solid (dashed) contours. Background grid is as in Fig. 4. (b) Cross section of isobaric temperature advection for the ahead 0-h composite as in (a) along $y = -100$ km.

The upper levels of the behind composite (Figs. 14c,d) were dominated by southwesterly flow with the strongest winds in quadrant B. A 40 m s^{-1} wind maximum was located at the northern edge of the composite at the upper levels, placing the portion of quadrant B nearest the inverted trough along the right side of a jet entrance region. At the level of maximum divergence, which is 200 hPa in this case (Fig. 16), two maxima were noted within quadrant B. The northernmost one was consistent with implied ascent in the Uccellini and

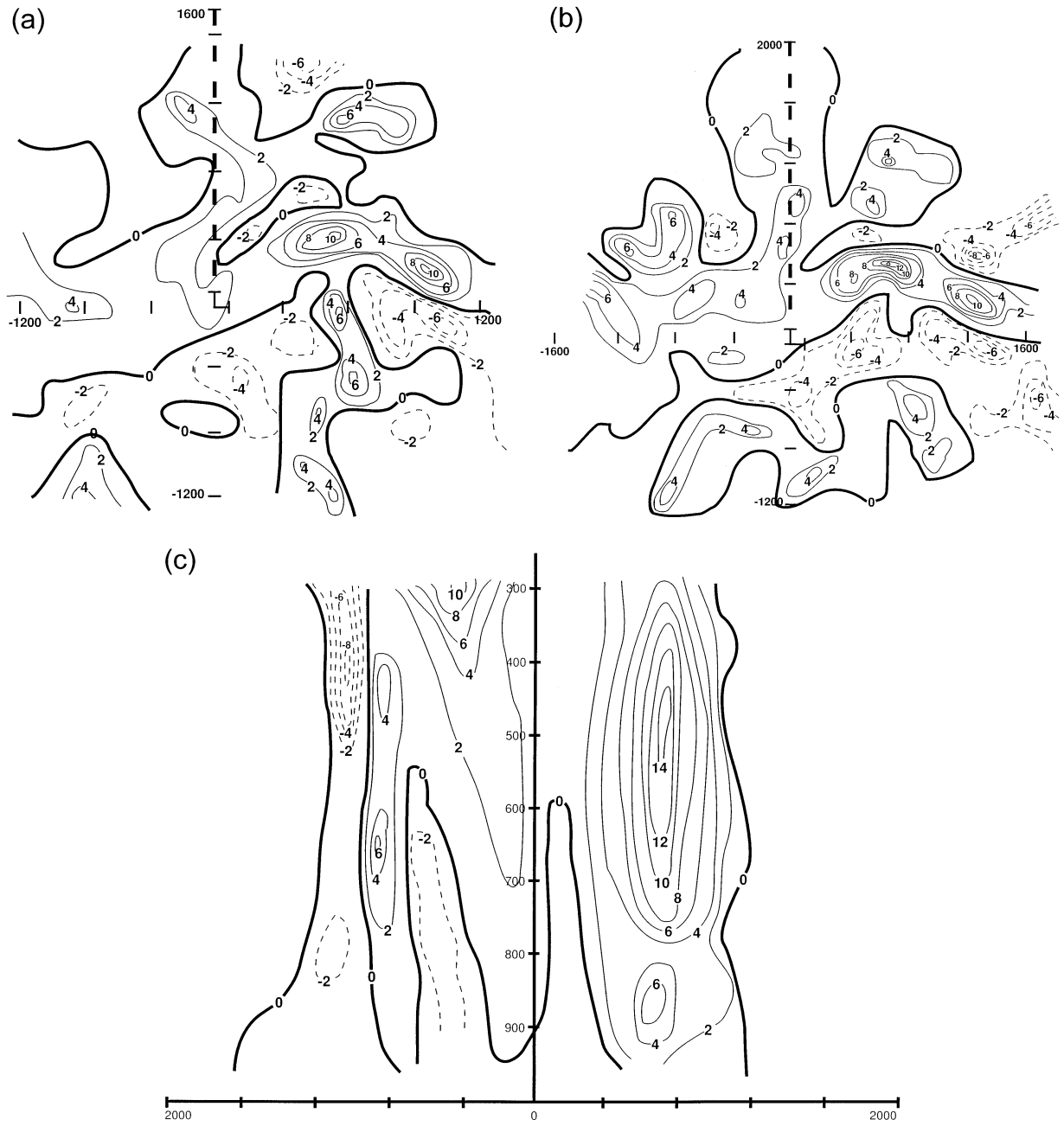

FIG. 10. Two-dimensional Miller (1948) upper-level frontogenesis (10^{-10} K m s^{-1}) for the ahead 0-h composites at (a) 700 and (b) 500 hPa. Solid (dashed) contours denote frontogenesis (frontolysis). Background grid is as in Fig. 4. (c) Cross section of upper-level frontogenesis as in (a) and (b) along $y = 400$ km.

Johnson (1979) model, while the southern one was located closer to the surface cyclone/frontal wave. The axis connecting the two maxima was located nearly directly above the frontogenesis maximum in the lower troposphere. Again, the collocation of these two processes was noted as a key difference for cyclones with inverted troughs in K94.

The 300-hPa relative vorticity advection field (Fig. 17a) was noisier than in the ahead cases but showed the strongest implied ascent in quadrant B. The cross section of relative vorticity advection (Fig. 17b) exhibited two columns containing an upward increase of cyclonic vorticity advection within quadrant B.

4. Discussion

The application of the composite technique to the analysis of the inverted trough cases did pose limita-

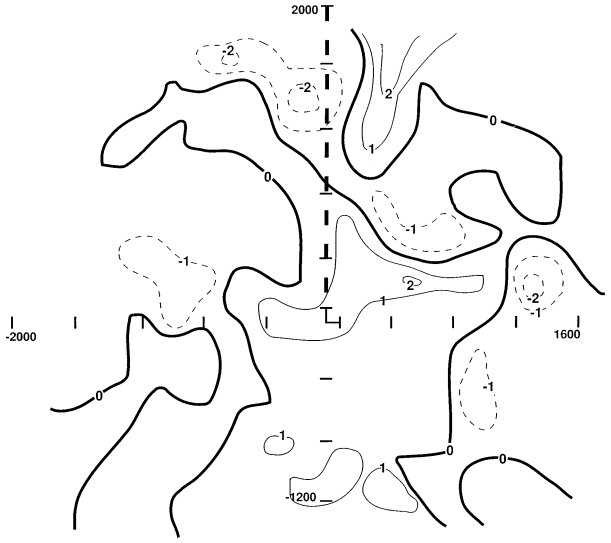

FIG. 11. Divergence (10^{-5} s^{-1}) for the ahead 0-h composite at 300 hPa. Solid (dashed) lines indicate divergence (convergence). Background grid is as in Fig. 4.

tions. Some signal damping did occur, so direct comparison of fields at the same time period between the ahead and behind cases was not always possible. One factor was the limited number of ''clean'' behind time periods in the 6-yr dataset. However, the behind results were consistent with the composite findings of K94, indicating that the composite in the current study is representative of inverted trough conditions. In addition, the small number of cases did result in composites that demonstrated clear differences between the ahead and behind cases. These differences were later confirmed in the case study work that will be presented in a future paper.

The second problem was dealing with the modest cyclogenesis associated with many inverted trough cases. The low signal-to-noise ratio in these cases makes analysis difficult. However, the operational forecaster must deal more frequently with more modest features like the bulk of inverted trough cases. The synoptic climatology of inverted trough cases performed in section 2 has shown that these systems are a frequent problem for central U.S. forecasters. An average of nearly 41 cases per season was found for the central United States. The winter and spring months averaged four cases per month during the study. Thus, the need for improved conceptual models for operational forecasters is demonstrated. Despite its limitations, the composite analysis did accomplish its goal by demonstrating a distinct difference at the synoptic scale between the ahead and behind cases.

A summary of the key processes and their different locations at 0 h is seen in Fig. 18. Both ahead and behind cases involved strong lower-tropospheric warm-air advection. However, the behind cases had a stronger ridge in quadrant A. The presence of this ridge forced the warm-air advection into quadrant B and elongated it parallel to the inverted trough within quadrant B. The presence of strong ridging ahead of the inverted trough was noted by K94 in the composite portion of their study. Quadrant B was also located within the entrance region of a jet streak along the northern fringe of the composite. Much of this area was within the right entrance region, which was favored for induced ascent (Uccellini and Johnson 1979), but the divergent area stretched across the whole entrance region. The region of maximum warm advection was located to the south of the divergence maximum, but the lower-tropospheric flow did progress to the jet entrance region and then turned underneath the jet, indicating some kind of link between the two processes. Once again, the results of K94 were found to be consistent with the behind cases in this study.

In contrast, the vertical nature of the ahead streamline trough prevented the warm-air advection from wrapping behind the surface low. This was true throughout all pretrough time periods. Thus, the surface inverted trough delineated the boundary between cold-air advection in quadrant B and warm-air advection in quadrant A. There was weak frontogenesis and, therefore, lift along the inverted trough, but the frontogenesis did not extend beyond the inverted trough. This is consistent with the empirical observation that passage of the inverted trough brought an end to the precipitation in ahead cases. However, the primary axis of warm-air advection and frontogenesis was near the x axis. This would be the location of the classic Norwegian cyclone warm front. Thus, the primary warm front in ahead cases was consistent with the Norwegian cyclone model, in contrast to the findings of K94.

In the ahead composite, the jet streak was located above the surface cyclone/frontal wave. So, the area of maximum divergence was primarily to the northeast of the surface cyclone in quadrant A. This location was also directly above the region of maximum warm-air advection and frontogenesis in the lower troposphere.

One should not expect these composite results to represent the entire conceptual model of ahead and behind cases. The case studies to be performed in a future paper will further illustrate the details of the circulation. However, the composites do show that the key processes differ substantially in location from previous models used to explain precipitation associated with central U.S. cold-season cyclones. The Norwegian cyclone model (Bjerknes 1919; Bjerknes and Solberg 1922) does include the possibility of an inverted trough. However, the Norwegian cyclone model does not include the possibility that the inverted trough could either separate two air masses, as is true in the behind cases, or mark the western edge of the dynamically forced ascent, as it does in the ahead cases.

The STORM (e.g., Hobbs et al. 1996) identified three major features missing from the Norwegian cyclone model, but none of them included an inverted trough.

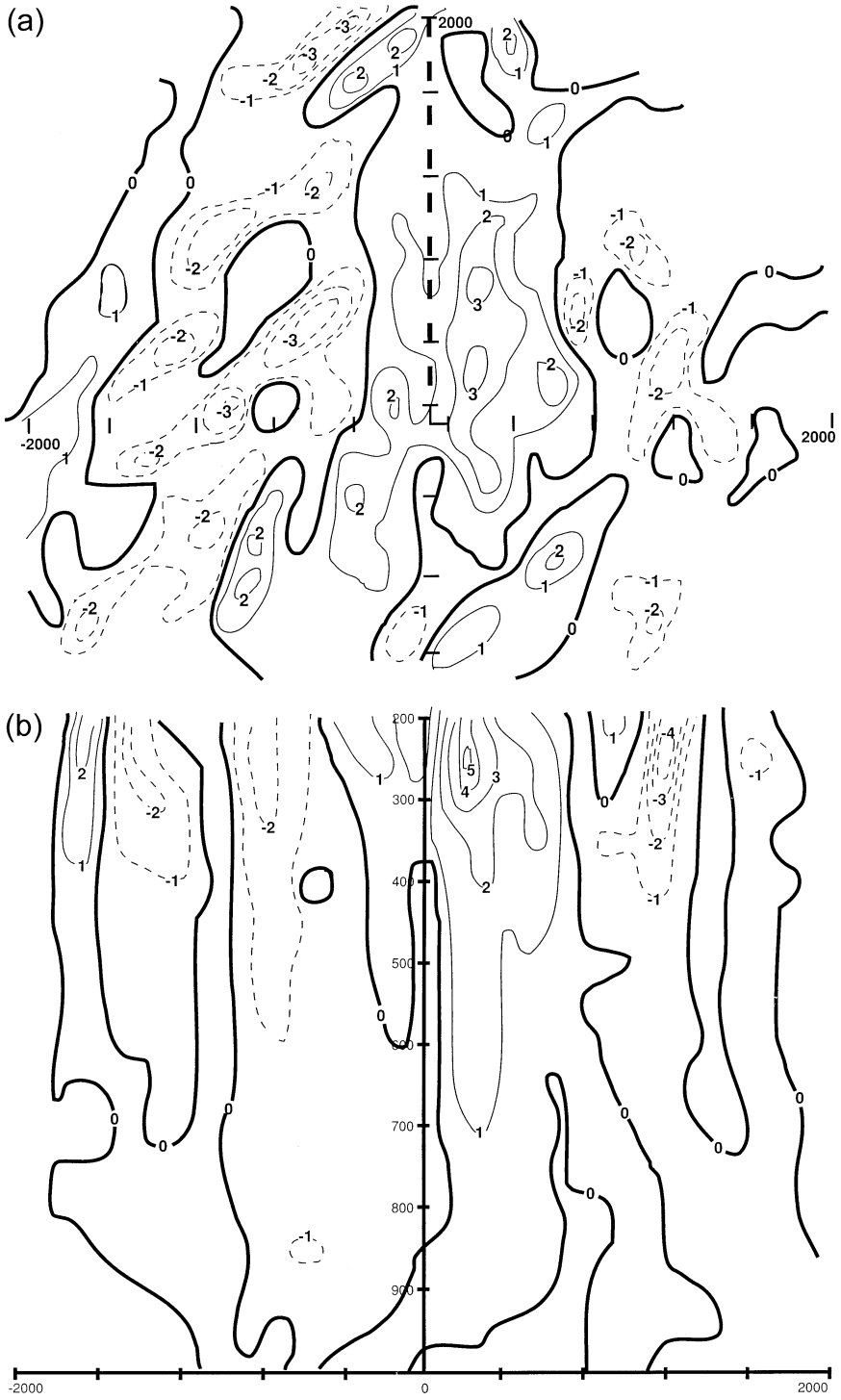

FIG. 12. (a) Relative vorticity advection (10^{-9} s^{-2}) for the ahead 0-h composite at 300 hPa. Solid (dashed) contours indicate cyclonic (anticyclonic) vorticity advection. Background grid is as in Fig. 4. (b) Cross section of isobaric relative vorticity advection for the ahead 0-h composite along $y = 300$ km as in (a).

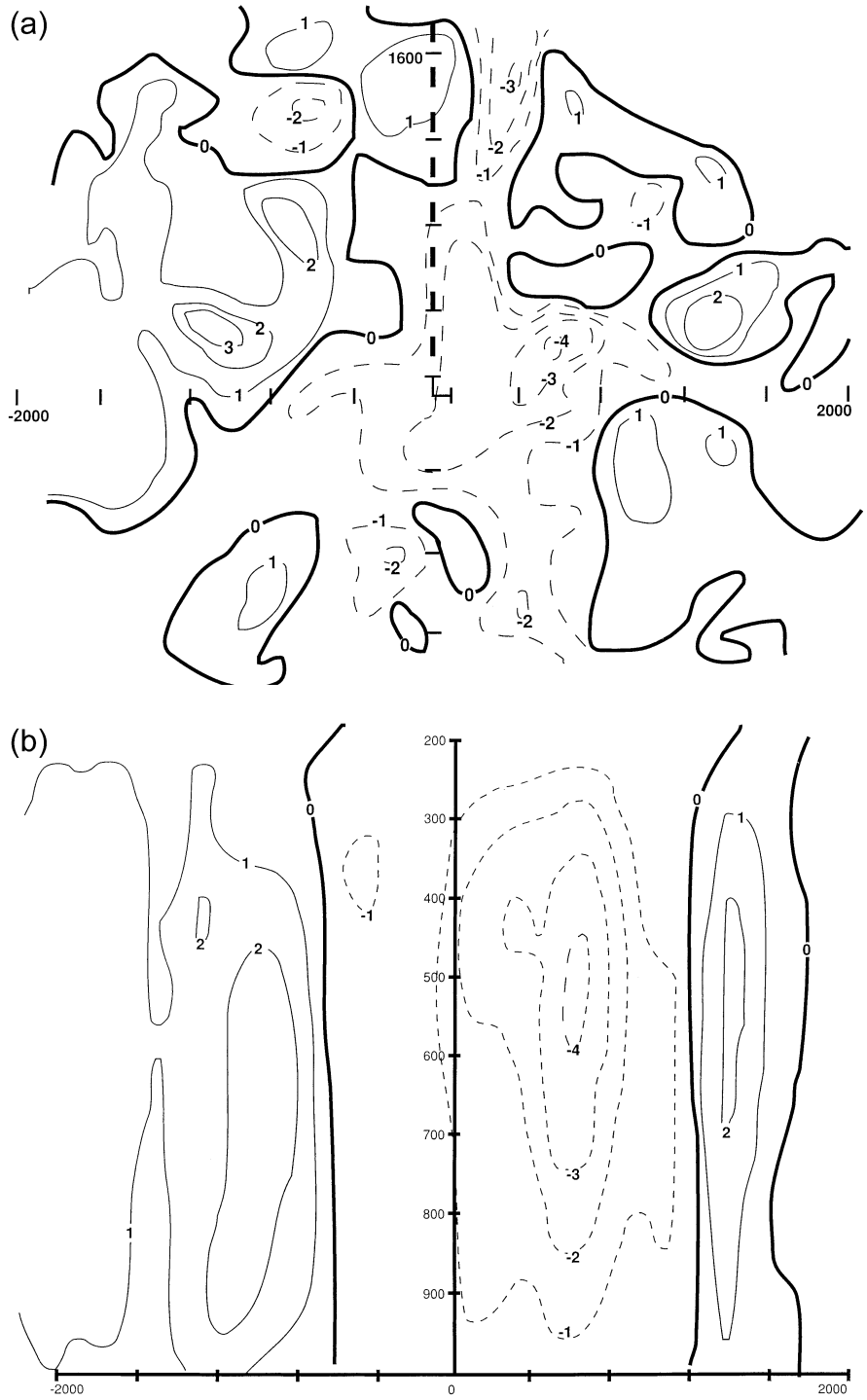

FIG. 13. (a) Kinematic vertical velocity (μbar s^{-1}) at 500 hPa for the ahead 0-h composite. Solid (dashed) contours indicate descent (ascent). Background grid is as in Fig. 4. (b) Cross section of kinematic vertical velocity for the ahead 0-h composite along $y = 200$ km as in (a).

The STORM allows for the possibility of precipitation in the northern sector of the cyclone as a result of (a) warm-air advection and frontogenesis along and on the cold side of the surface arctic front, or (b) the northward progression of the pre-dry-trough rainband. The activity of the arctic front is consistent with the ahead cases for this study. However, the pre-dry-trough rainband would begin as convection along the dry trough of the cyclone,

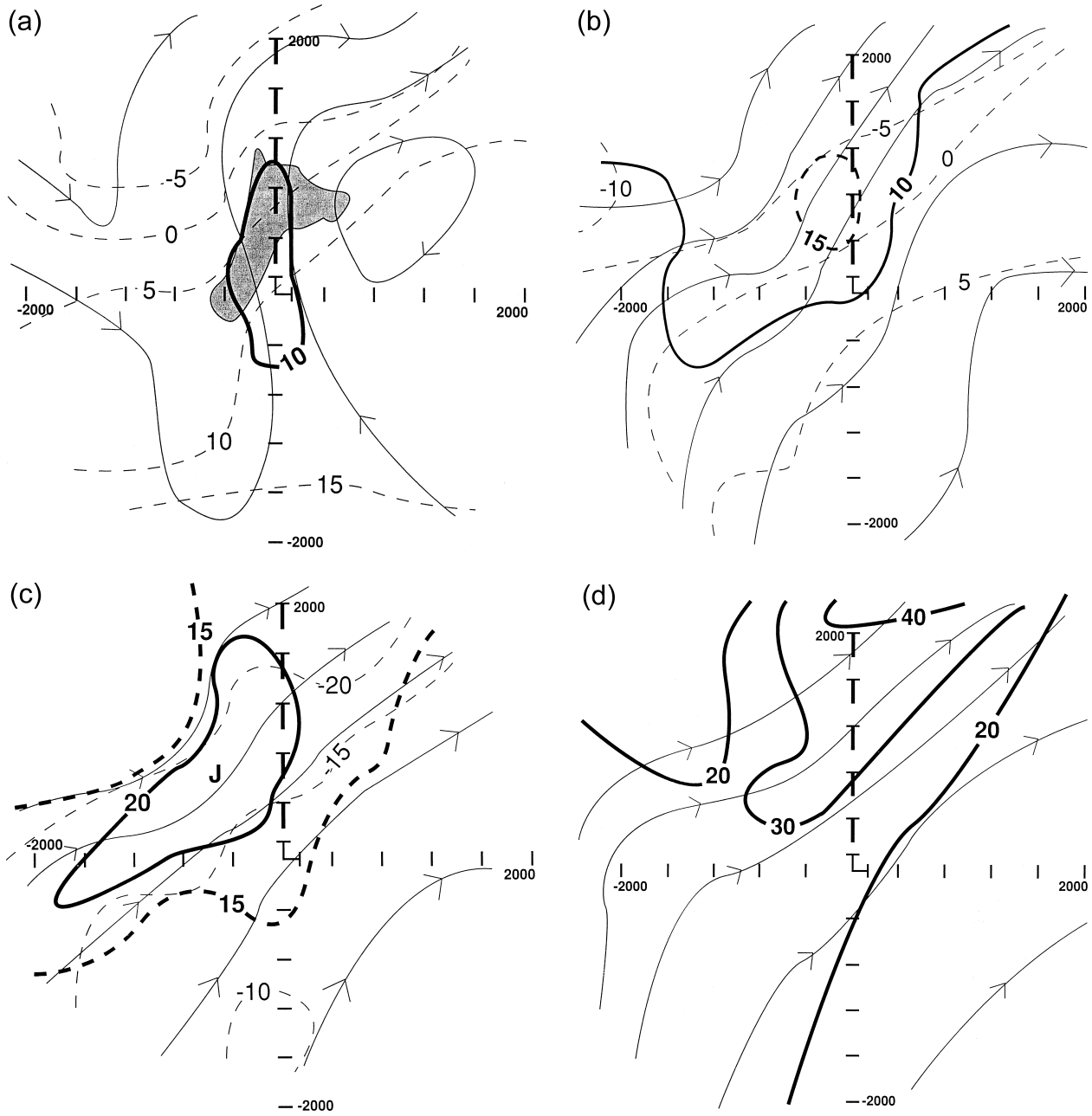

FIG. 14. Composite behind 0-h isobaric analysis as in Fig. 4 at (a) 850, (b) 700, (c) 500, and (d) 300 hPa. Note that the stippled area at 850 hPa indicates areas with a dewpoint depression of ≤5°C. The lack of stippling in (b)–(d) indicates that all areas have a dewpoint depression >5°C.

which is within the warm sector. It is possible that such convection would eventually develop within inverted trough cases. However, the STORM does not mention why the ascent would be favored to the west of the inverted trough in a behind case or to the east in an ahead case. The STORM, in contrast, simply denotes the continuing northward movement of the rainband into the cold sector without any preference to the northwest or northeast flank of the cyclone.

The conceptual model proposed by K94 appears to fit the behind cases but excludes the ahead cases. This is likely the result of the different criteria for selecting cases. K94 required that a temperature change of at least 5°C be present across the inverted trough, while the synoptic climatology performed in this study did not make such a requirement. The behind composites show that frontogenesis does occur along the inverted trough in the lower troposphere; thus, the inverted trough becomes the functional surface warm front, a departure from the typical warm front on the eastern edge of a

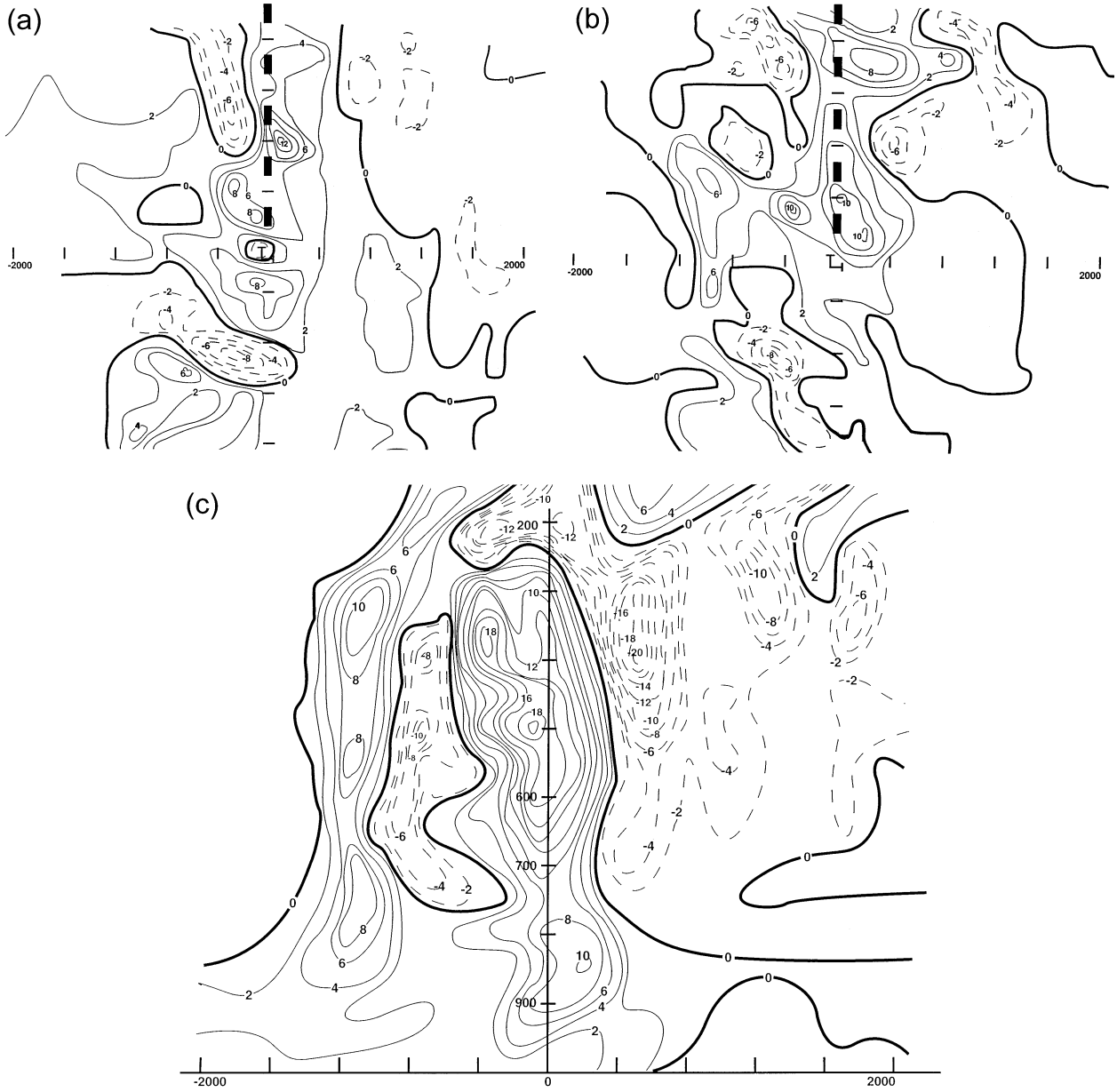

FIG. 15. Isobaric temperature advection for the behind 0-h composite as in Fig. 9a at (a) 850 and (b) 700 hPa. (c) Cross section of isobaric temperature advection for the behind 0-h composite along $y = 700$ km as in (a) and (b).

Norwegian cyclone. K94 showed, in fact, that the inverted trough marked the boundary between an old, modified arctic air mass and a fresh supply of arctic air with the modified air overrunning the new cold air. However, by requiring a temperature gradient across the inverted trough, K94 could only diagnose those cases in which the inverted trough was a front.

However, no temperature gradient was noted across the inverted trough during the ahead cases. Instead, the lack of tilt with height of the streamline trough made the inverted trough the boundary between cold-air and warm-air advection. This orientation seems to be linked to the lack of precipitation behind the inverted trough. The authors do not preclude the possibility that the inverted trough could develop a baroclinic structure later. K94 did note in their case studies that four or five air masses were seen during the early stages of cyclogenesis. As cyclogenesis proceeded, some of these fronts merged. Also, one of K94's case studies initially had two surface inverted troughs, which later merged. In this study, however, the inverted trough remained as a surface pressure system without becoming associated with a temperature gradient.

The most important contribution of the present work

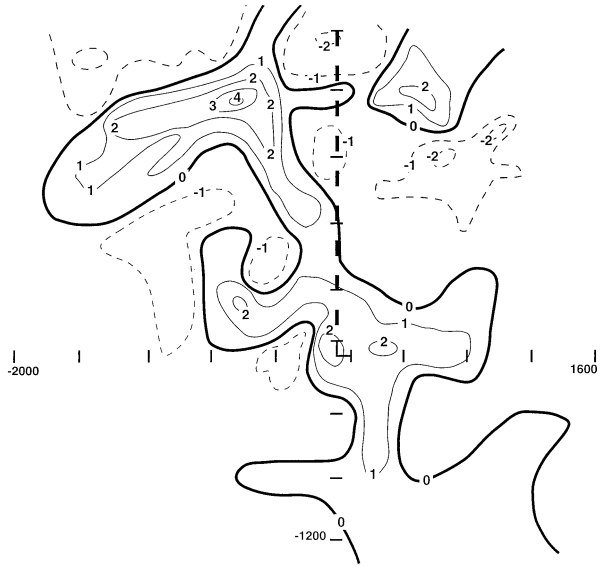

FIG. 16. Divergence for the behind 0-h composite at 200 hPa as in Fig. 11.

is the addition of a second conceptual model, the ahead precipitation distribution, for the operational forecasting of inverted trough storms in the central United States. The authors' operational forecast experience has shown that the standard NCEP models are able to predict the presence of inverted troughs and that the forecast precipitation fields often denote the difference between ahead and behind cases. However, forecasters who are unaware of the possible modification of the precipitation signal by the processes associated with inverted troughs can reject the model forecast and substitute a precipitation distribution more commonly associated with the Norwegian cyclone model (Bjerknes 1919; Bjerknes and Solberg 1922). In contrast, the Sioux Falls National Weather Service Forecast Office has been using these conceptual models to successfully forecast both the clean inverted trough cases and some of their hybrids since this research began. Hopefully, publication of these results will allow more operational forecasters to use this conceptual model to improve their ability to forecast precipitation associated with inverted trough cases.

Last, note that QG dynamic reasoning was relatively successful in diagnosing the support for ascent in these composites, despite the fact that this approximation does not always handle frontogenesis or jet dynamics well (e.g., Moore and VanKnowe 1992). If the signal-to-noise ratio had been higher, the application of **Q** vectors (Hoskins et al. 1978; Hoskins and Pedder 1980) probably would have been successful. However, these cases illustrated the pitfalls encountered by the use of 500-hPa positive vorticity advection (PVA), a simplification often used in the application of QG dynamics. In fact, the 500-hPa composite field is modest in all respects, except for the kinematically calculated ascent, which depends on the divergence field throughout the column. The PVA method failed since the largest values of warm-air advection and frontogenesis were found in the lower troposphere and the largest values of cyclonic vorticity advection were involved with the jet streak circulations in the upper troposphere. Thus, inverted trough cases remind operational forecasters that it is the upward increase of cyclonic vorticity advection that forces ascent in the QG omega equation. This can sometimes be approximated by PVA at 500 hPa, but not in all cases. The failure of the PVA simplification will also be documented by case studies in future work. In contrast, the case studies will document the utility of isentropic potential vorticity analysis in the identification of wave interaction during inverted trough cases.

5. Conclusions

Cold-season inverted troughs in the central United States have been shown to modify the precipitation distribution associated with the Norwegian cyclone model in two major ways. Ahead cases, which composed 103 of the 247 cases found in a six-season study, produce precipitation between the inverted trough and the conventional warm front. In the ahead composites, all of the warm-air advection and lower-tropospheric frontogenesis takes place to the east of the inverted trough within quadrant A. Thus, the classic Norwegian cyclone model surface warm front remains active. Cold-air advection and subsidence occur behind the inverted trough, since the trough in the wind field remains vertically stacked. The ahead cases tend to be more progressive because of the presence of a nearly zonal jet maximum over the center of the surface cyclone. The upward increase in cyclonic vorticity advection is also consistent with the ascent found to the east of the inverted trough.

The behind cases, which contributed only 21 of the 247 cases in a six-season climatology but are responsible for some of the most notorious northern plains snowfalls, produce the bulk of their precipitation to the west of the inverted trough. The composite study demonstrated that behind cases are dominated by split flow with much stronger ridging ahead of the cyclone and inverted trough. The phasing of warm-air advection between the two streams rotates the lower-tropospheric isotherms parallel to the inverted trough, transforming the inverted trough into the dominant warm front. In contrast, the conventional warm front is never a focus of ascent. The dominance of the southern stream in the split flow produces the divergent branch of the circulation about a jet entrance region to also develop over quadrant B, reinforcing the lift. The results of the behind cases correlate well with those examined by K94, but the ahead cases compose a new category.

Acknowledgments. Plotting and analysis for the composites were performed by Eric Green, Wendilyn Kau-

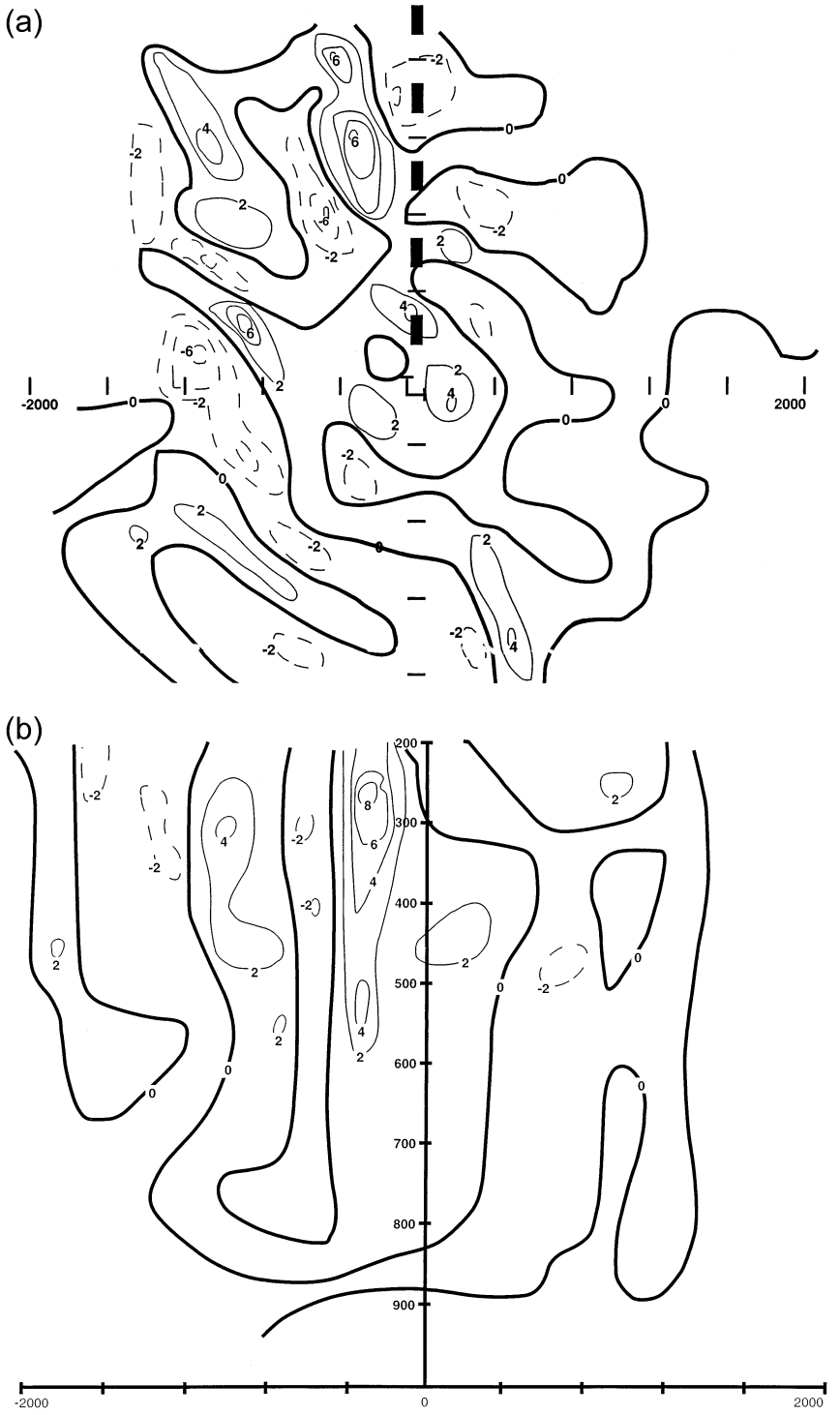

FIG. 17. (a) Isobaric relative vorticity advection for the behind 0-h composite as in Fig. 11a at 300 hPa. (b) Cross section of isobaric relative vorticity advection for the behind 0-h composite along $y = 1100$ km as in Fig. 15a.

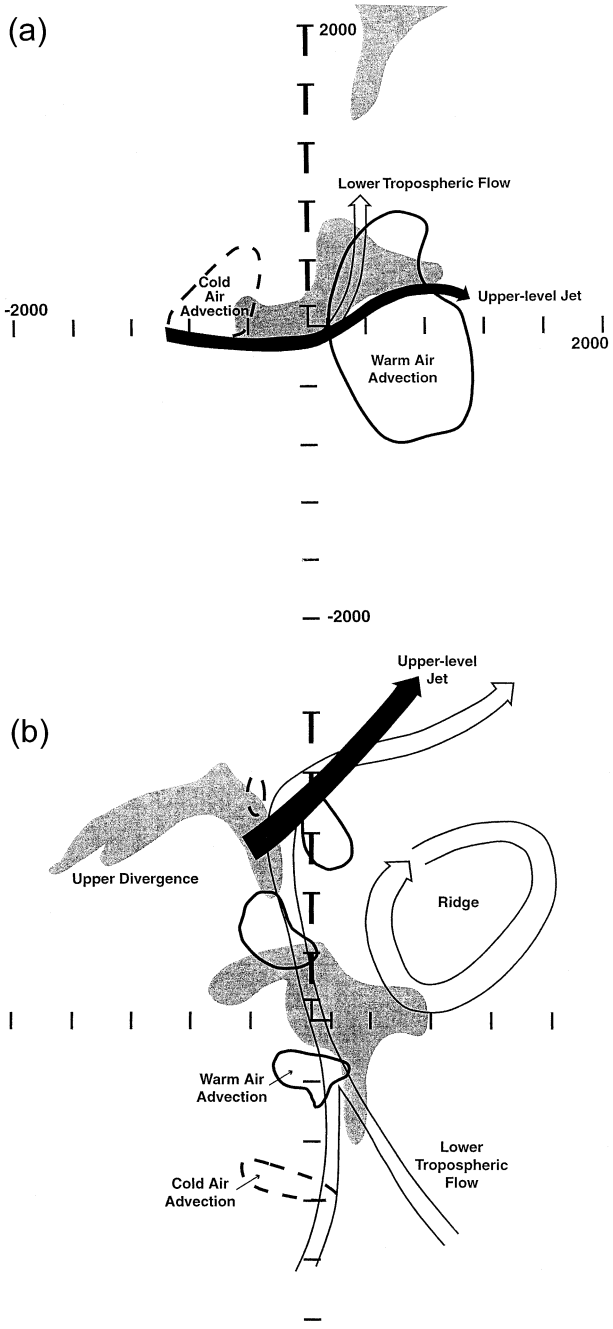

FIG. 18. Location of key processes for (a) ahead 0-h composite, and (b) behind 0-h composite. Open (solid) arrow denotes representative lower-tropospheric (upper tropospheric) streamline. Solid (dashed) contour encloses region in which warm-air (cold air) advection exceeds 6×10^{-8} K s^{-1}. Stippling indicates region in which upper-tropospheric divergence exceeds 1×10^{-5} s^{-1}. Background grid is as in Fig. 4.

feld, David King, and Jason Kluver as well as the coauthors. Drafting of the figures was done by Mary Shrode, Noah Wentz, and Kaori Hamamoto. The comments of the three anonymous reviewers substantially improved the text. This research was supported by National Science Foundation Grant ATM-9610356. Some conclusions in this paper were drawn from the research in the companion paper that was supported by the COMET Partners Project, Grant UCAR S98-90782.

REFERENCES

Barnes, S. L., 1964: A technique for maximizing details in numerical weather map analysis. *J. Appl. Meteor.*, **3,** 396–409.

——, 1973: Mesoscale objective analysis using weighted time-series observations. NOAA Tech. Memo. ERL NSSL-62, 60 pp. [NTIS COM-73-10781.]

Bellamy, J. C., 1949: Objective calculations of divergence, vertical velocity, and vorticity. *Bull. Amer. Meteor. Soc.*, **30,** 45–49.

Bjerknes, J., 1919: On the structure of moving cyclones. *Geofys. Soc.*, **1,** 1–8.

——, and H. Solberg, 1922: Life cycle of cyclones and polar front theory of atmospheric circulation. *Geofys. Publ.*, **3,** 1–18.

Bluestein, H. B., 1986: Fronts and jet streaks: A theoretical perspective. *Mesoscale Meteorology and Forecasting*, P. S. Ray, Ed., Amer. Meteor. Soc., 173–215.

Hobbs, P. V., J. D. Locatelli, and J. E. Martin, 1996: A new conceptual model for cyclones generated in the lee of the Rocky Mountains. *Bull. Amer. Meteor. Soc.*, **77,** 1169–1178.

Hoskins, B. J., and M. A. Pedder, 1980: The diagnosis of middle latitude synoptic development. *Quart. J. Roy. Meteor. Soc.*, **106,** 707–719.

——, I. D. Draghici, and H. C. Davies, 1978: A new look at the omega equation. *Quart. J. Roy. Meteor. Soc.*, **104,** 31–38.

Keshishian, L. G., L. F. Bosart, and W. E. Bracken, 1994: Inverted troughs and cyclogenesis over interior North America: A limited regional climatology and case studies. *Mon. Wea. Rev.*, **122,** 565–607.

Keyser, D., M. J. Reeder, and R. J. Reed, 1988: A generalization of Pettersen's frontogenesis function and its relation to the forcing of vertical motion. *Mon. Wea. Rev.*, **116,** 762–780.

Lackmann, G. M., L. F. Bosart, and D. Keyser, 1996: Planetary- and synoptic-scale characteristics of explosive wintertime cyclogenesis over the western North Atlantic Ocean. *Mon. Wea. Rev.*, **124,** 2672–2702.

Miller, J. E., 1948: On the concept of frontogenesis. *J. Meteor.*, **5,** 169–171.

Moore, J. T., and G. E. VanKnowe, 1992: The effect of jet-streak curvature on kinematic fields. *Mon. Wea. Rev.*, **120,** 2429–2441.

Mullen, S. L., and D. P. Baumhefner, 1988: Sensitivity of numerical simulations of explosive oceanic cyclogenesis to changes in physical parameterizations. *Mon. Wea. Rev.*, **116,** 2289–2329.

Murtha, D. D., and D. J. Blondin, 1995: A study of the Thanksgiving 1993 snowstorm—Enhancement of heavy snow over northeast South Dakota in response to tropopause undulation. Preprints, *Fourth National Weather Workshop*, Kansas City, MO, National Weather Service Central Region, 17.

O'Brien, J. J., 1970: Alternative solutions to the classical vertical velocity problem. *J. Appl. Meteor.*, **9,** 197–203.

Uccellini, L. W., and D. R. Johnson, 1979: The coupling of upper and lower tropospheric jet streaks and implications for the development of severe convective storms. *Mon. Wea. Rev.*, **107,** 682–703.

Weisman, R. A., K. G. McGregor, and P. N. Schumacher, 1998: Precipitation regimes during cold-season inverted trough cases in the central U.S. Preprints, *16th Conference on Weather Analysis and Forecasting*, Norfolk, VA, Amer. Meteor. Soc., 374–376.